The 12th Symposium on Polar Science
15 – 18 November 2021

National Institute of Polar Research
Research Organization of Information and Systems

Session IW
Whole atmosphere

Program and Abstracts

Conveners
Yoshihiro Tomikawa, Mitsumu K. Ejiri, and Takanori Nishiyama (NIPR)

【IW】Whole atmosphere

Scopes

This session provides an opportunity to present and discuss observational, theoretical, and modeling studies focusing on a variety of phenomena in each layer or across multiple layers of the earth's atmosphere.

Conveners : **Yoshihiro Tomikawa, Mitsumu K. Ejiri, and Takanori Nishiyama (NIPR)**

Real-time Oral presentations (14:00 – 16:30)

Date: Tue. 16 November

Note: [I] represents an invited talk.

Chair: Masaru Kogure (Kyushu Univ.)				
IWo01	14:00 - 14:30	[I] Characterization of atmospheric turbulence at Syowa station from Datahawk UAVs, stratospheric balloons and the PANSY radar	*Luce, Hubert (RISH, Kyoto Univ.), Abhiram Doddi (Global Atmospheric Technologies and Sciences), Dale Lawrence (Department of Aerospace Engineering Sciences, Univ. of Colorado), Tyler Mixa (Global Atmospheric Technologies and Sciences), Masanori Yabuki (RISH, Kyoto Univ.), Koji Nishimura (RISH, Kyoto Univ.), Hiroyuki Hashiguchi (RISH, Kyoto Univ.)	IWo01_Luce_00531_01.pdf
IWo02	14:30 - 14:45	Kelvin-Helmholtz billows detected by the PANSY radar in the Antarctic troposphere and lower stratosphere	*Minamihara, Yuichi (The Univ. of Tokyo), Kaoru Sato (The Univ. of Tokyo), Masaki Tsutsumi (NIPR & SOKENDAI)	IWo02_Minamihara_00184_01.pdf
IWo03	14:45 - 15:00	Characteristics and reproducibility of inertia gravity waves over Syowa Station ~Comparison between the PANSY radar and the ERA5 reanalysis~	*Yoshida, Lihito (SOKENDAI), Yoshihiro Tomikawa (NIPR & SOKENDAI), Mitsumu K. Ejiri (NIPR & SOKENDAI), Masashi Kohma (The University of Tokyo), Kaoru Sato (The University of Tokyo)	IWo03_Yoshida_00190_01.pdf
IWo04	15:00 - 15:15	Contribution of gravity waves to the universal vertical wavenumber (m^-3) spectra revealed by a gravity-wave permitting general circulation model	*Okui, Haruka (The Univ. of Tokyo), Kaoru Sato (The Univ. of Tokyo), Shingo Watanabe (JAMSTEC)	IWo04_Okui_00268_01.pdf
Chair: Taishi Hashimoto (NIPR)				
IWo05	15:15 - 15:30	Gravity Wave Weakening in the 2019 Antarctic Stratospheric Sudden Warming	*Kogure, Masaru (Department of Earth and Planetary Science, Kyushu Univ.), Jia Yue (NASA Goddard Space Flight Center), Huixin Liu (Department of Earth and Planetary Science, Kyushu Univ.)	IWo05_Kogure_00467_02.pdf
IWo06	15:30 - 15:45	An event study on sporadic Fe layer at Syowa station (69.0°S, 39.6°E) based on numerical simulation and simultaneous observation of Fe density and wind	*Nishiyama, Takanori (NIPR & SOKENDAI), Mitsumu K. Ejiri (NIPR & SOKENDA), Takuo T. Tsuda (The University of Electro- Communications), Katsuhiko Tsuno (ASI, RIKEN), Takuji Nakamura (NIPR & SOKENDA), Masaki Tsutsumi (NIPR & SOKENDA), Makoto Abo (Tokyo Metropolitan University), Taku D. Kawahara (Shinshu University), Takayo Ogawa (ASI, RIKEN), Satoshi Wada (ASI, RIKEN)	IWo06_Nishiyama_00166_01.pdf
IWo07	15:45 - 16:00	An advanced meteor wind study based on MF radar observations over Syowa (69S,39E), Antarctic	*Tsutsumi, Masaki (NIPR & SOKENDAI), Taishi Hashimoto (NIPR & SOKENDAI), Koji Nishimura (RISH, Kyoto Univ.), Toru Sato (ILAS, Kyoto Univ.), Masashi Kohma (The Univ. of Tokyo), Kaoru Sato (The Univ. of Tokyo)	IWo07_Tsutsumi_00371_01.pdf
IWo08	16:00 - 16:30	[I] High altitude meteors detected by the interferometric MU radar	*Kastinen, Daniel (Swedish Institute of Space Physics), Johan Kero (Swedish Institute of Space Physics)	IWo08_Kastinen_00491_01.pdf

Real-time Poster presentations (16:40 – 18:00)

Date: Tue. 16 November

	16:40 - 16:45	1-minute poster appeal (5 short talks of IWp1 – IWp5)
	16:45 - 18:00	Poster session core time

Real-time Oral presentations (9:00 – 10:45)

Date: Wed. 17 November

Chair: Mitsumu K. Ejiri (NIPR)				
IWo09	09:00 - 09:30	[I] Developing the NASA Atmospheric Waves Experiment (AWE)	Taylor, M. J. (Utah State Univ.), J. M. Forbes(Univ. of Colorado), D. C. Fritts (GATS), *J. B. Snively (Embry Riddle Aeronautical Univ.), S. D. Eckermann (Naval Research Laboratory), H.-L. Liu (NCAR), P.-D. Pautet (Utah State Univ.), Y. Zhao (Utah State Univ.), E. Syrstad (Utah State Univ., Space Dynamic Laboratory), R. Esplin (Utah State Univ., Space Dynamic Laboratory), B. Lamborn (Utah State Univ., Space Dynamic Laboratory), H. Latvakoski (Utah State Univ., Space Dynamic Laboratory)	IWo09_Taylor_00258_01.pdf
IWo10	9:30 - 9:45	Airglow observations from International Space Station by ISS-IMAP/VISI	*Saito, A. (Kyoto Univ.), T. Sakanoi (Tohoku Univ.), Y. Hozumi (NICT), S. Perwitasari (NICT)	IWo10_Saito_00454_01.pdf
IWo11	9:45 - 10:00	Characteristics of gravity wave horizontal phase velocity spectra in the mesosphere over the Antarctic stations, Syowa and Davis.	*Kogure, Masaru (Kyushu Univ.), Takuji Nakamura (NIPR & SOKENDAI), Damian J. Murphy (AAD), Michael J. Taylo (Utah State Univ.)r, Yucheng Zhao (Utah State Univ.), Pierre-Dominique Paute (Utah State Univ.), Masaki Tsutsumi (NIPR & SOKENDAI), Yoshihiro Tomikawa (NIPR & SOKENDAI), Mitsumu K. Ejiri (NIPR & SOKENDAI), Takanori Nishiyama (NIPR & SOKENDAI)	IWo11_Kogure_00467_01.pdf
IWo12	10:00 - 10:15	Propagation direction analysis of medium-scale traveling ionospheric disturbances (MSTIDs) observed with 2D GPS-TEC map using three-dimensional spectral analysis method over North America	*Perwitasari, Septi (NICT), Takuji Nakamura (NIPR & SOKENDAI), Takuya Tsugawa (NICT), Michi Nishioka (NICT), Yoshihiro Tomikawa(NIPR & SOKENDAI), Mitsumu K. Ejiri (NIPR & SOKENDAI), Masaru Kogure (Kyushu University), Yuichi Otsuka (Nagoya Univ.), Atsuki Shinbori (Nagoya Univ.), Hidekatsu Jin (NICT), Chihiro Tao (NICT)	IWo12_Perwitasari_00523_01.pdf
IWo13	10:15 - 10:30	Multi-wavelength auroral imaging observation with attitude-stabilized all-sky imagers on Shirase	*Sakanoi, Takeshi(Tohoku University), Yamashina, Saki (Kyoto University), Hozumi, Yuta (NICT), Tsuda, Takuo T., Aoki, Takeshi (The University of Electro-Communications), Naoi, Takahiro, Nagahara, Masato (NICT), Saito, Akinori (Kyoto University), Ejiri, Mitsumu K., Nishiyama, Takanori (NIPR)	IWo13_Sakanoi_00590_01.pdf
IWo14	10:30 - 10:45	Citizen science of aurora hunting in Japan: Evidence of red aurora on October 12, 2021	*Kataoka, Ryuho (NIPR & SOKENDAI)	IWo14_Kataoka_00210_02.pdf

Poster presentations (16 November - 18 November, Real-time presentation: 16 November 16:45 - 18:00)

IWp1	ANGWIN: ANtarctic Gravity Wave Instrument Network	*Murphy, Damian (AAD), Tracy Moffat-Griffin (BAS), Takuji Nakamura (NIPR & SOKENDAI), Jose Valentin Bageston (National Institute for Space Research INPE), Geonhwa Jee (Korea Polar Research Institute), Michael J. Taylor (Utah State Univ.)	IWp01_Murphy_00605_01.pdf
IWp2	Polar mesospheric cloud detection by the Advanced Himawari Imager onboard the Japanese geostationary-Earth-orbit meteorological satellite Himawari-8	*Tsuda, Takuo T. (UEC), Yuta Hozumi (NICT), Yoshiaki Ando (UEC), Keisuke Hosokawa (UEC), Hidehiko Suzuki (Meiji Univ.), Takeshi Murata (NICT), Takuji Nakamura (NIPR), Jia Yue (NASA), Kim Nielsen (UVU), Yasunobu Miyoshi (Kyushu Univ.)	IWp02_Tsuda_00085_01.pdf
IWp3	Development of image correction system for the all-sky imager onboard Antarctic Research Vessel "Shirase"	*Yamashina, Saki (Kyoto Univ.), Akinori Saito (Kyoto Univ.), Takeshi Sakanoi (Tohoku University), Yuta Hozumi (NICT), Takuo T. Tsuda (UEC), Takeshi Aoki (UEC), Takahiro Naoi (NICT), Masato Nagahara (NICT), Mitsumu K. Ejiri (NIPR & SOKENDAI), Takanori Nishiyama (NIPR & SOKENDAI)	IWp03_Yamashina_00597_01.pdf
IWp4	Characteristics of 8 hr and 6 hr atmospheric waves in the polar upper mesosphere and lower thermosphere derived by the sodium LIDAR at Tromsoe	*Morikawa, Chiaki, Nozawa, Satonori (Nagoya Univ.), Tsuda, Takuo T. (The University of Electro-Communications), Kawahara, Takuya (Shinshu University), Saito, Norihito, Wada, Satoshi (RIKEN, RAP), Takahashi, Toru (Electronic Navigation Research Institute)	IWp04_Morikawa_00177_01.pdf
IWp5	A long lived mesospheric Ca+ ion layer observed by a resonance scattering lidar at Syowa	*Ejiri, Mitsumu K. (NIPR & SOKENDAI), Takanori Nishiyama (NIPR & SOKENDAI), Takuo T. Tsuda (UEC), Masaki Tsutsumi, Takuji Nakamura (NIPR & SOKENDAI), Makoto Abo (Tokyo Metropolitan University), Katsuhiko Tsuno (RIKEN, RAP), Takuya D. Kawahara (Shinshu Univ.), Takayo Ogawa (RIKEN, RAP), Satoshi Wada (RIKEN, RAP)	IWp05_Ejiri_00258_01.pdf

Characterization of atmospheric turbulence at Syowa station from Datahawk UAVs, stratospheric balloons and the PANSY radar

Hubert Luce[1], Abhiram Doddi[2], Dale Lawrence[3], Tyler Mixa[2], Masanori Yabuki[1], Koji Nishimura[1], Hiroyuki Hashiguchi[1]

[1]*Research Institute for Sustainable Humanosphere, Kyoto University, Japan*
[2] *Global Atmospheric Technologies and Sciences, Boulder, Colorado, USA*
[3] *Department of Aerospace Engineering Sciences, University of Colorado, Boulder, USA*

Small-scale turbulence generated by convective and shear instabilities and gravity wave breaking strongly contributes to the vertical transport of matter and to the energy budgets of the atmosphere. In this regard, the PANSY radar is a unique tool for studying waves, instabilities and turbulence in the polar tropo-stratosphere (e.g. *Tomikawa et al., 2015; Kohma et al., 2019; Minamihara et al., 2020, Nishimura et al., 2020*). However, the characterization of turbulence from radar measurements remains a challenge because the radar data are still subject to interpretations and the models used to retrieve turbulence parameters are not fully validated (e.g., *Luce et al., 2018*). Building on results obtained from previous field campaigns (called ShUREX - Shigaraki UAV and Radar EXperiment 2015-2017) (*Kantha et al., 2017),* we propose a field campaign in the vicinity of the PANSY radar mainly with small and light Unmanned Aerial Vehicles (UAVs), called DataHawks (*Lawrence and Balsley, 2013*), and stratospheric balloons developed by Colorado University (Boulder, USA). They are equipped with high-resolution velocity and temperature sensors to measure turbulence kinetic energy dissipation rate ε and the temperature structure parameter C_T^2, among other fundamental parameters. The UAV and balloon flight configurations, schematically represented in Figure 1, will allow further radar performance assessment based on direct in-situ turbulence measurements. In addition, we propose to deploy the stratospheric balloons and the UAVs during Intensive Operation Periods (IOPs), in coordination with the LODEWAVE schedule, for additional information on waves and turbulence in the tropo-stratosphere. The membership of the UAV and balloon operators to GATS (Boulder, Colorado) will permit us to include a DNS modelling part.

Turbulent motions in the Atmospheric Boundary Layer (ABL) play a critical role in the vertical transport of sensible and latent heats and the formation of clouds, which in turn affect radiation budgets in polar regions. Therefore, in the background of the above-mentioned objectives, we will operate UAVs and possibly Tethered Lifting System (TLS) balloons equipped with turbulence sensors to sample the ABL and to observe its daily evolution for a better parameterization of the ABL in polar weather models.

This project is motivated by the will to share innovative and efficient tools to study the small-scale dynamics and structure of the lower atmosphere. Thanks to these technical and scientific experiences, we hope that we can bring a benefit to the studies with the PANSY radar and at the Syowa station in general, with the support of NIPR and associated institutes.

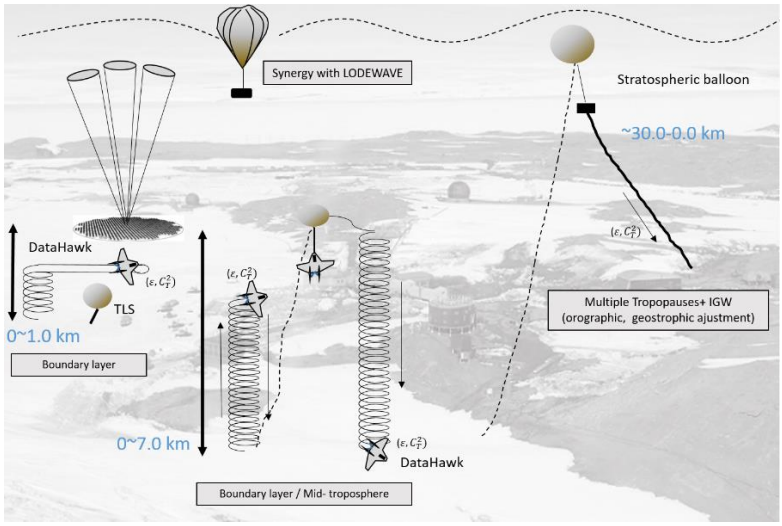

Figure 1. DataHawk UAVs and stratospheric balloons near the PANSY radar.

References

Kantha, L., D. Lawrence, H. Luce, H. Hashiguchi, T. Tsuda, R. Wilson T. Mixa, M. Yabuki, Shigaraki UAV-Radar Experiment (ShUREX 2015): an overview of the campaign with some preliminary results. Prog. Earth Planet Sci., 4:19, 2017.

Kohma, M., K. Sato, Y. Tomikawa, K. Nishimura and T. Sato, Estimate of turbulent energy dissipation rate from the VHF radar and radiosonde observations in the Antarctic, J. Geophys. Res., Atmosphere, 124, 2976-2993, 2019.

Lawrence, D., and B. B. Balsley, High-Resolution Atmospheric Sensing of Multiple Atmospheric Variables Using the DataHawk Small Airborne Measurement System, J. Atmos. Ocean. Tech., 30, 2352-2366, 2013.

Luce, H., L. Kantha, H. Hashiguchi, D. Lawrence and A. Doddi, Turbulence kinetic energy dissipation rates estimated from concurrent UAV and MU radar measurements, Earth. Plan. Space, 70:207, 2018.

Minamihara, Y., K. Sato, and M. Tsutsumi, Intermittency of gravity waves in the Antarctic troposphere and lower stratosphere revealed by the PANSY radar observation, J. Geophys. Res., Atmospheres, 125, 1-25, 2020.

Nishimura, K., M. Kohma, K. Sato and T. Sato, Spectral observation theory and beam debroadening algorithm for atmospheric radar, IEEE Trans. Geos. Rem. Sens., 58, 6767-6775, 2020.

Tomikawa, Y. et al., Vertical wind disturbances during a strong wind event observed by the PANSY radar at Syowa Station, Antarctica, Mon. Wea. Rev., 143, 1804-1821, 2015.

Kelvin-Helmholtz billows detected by the PANSY radar in the Antarctic troposphere and lower stratosphere

Y. Minamihra[1], K. Sato[1] and M. Tsutsumi[2]
[1]*Department of Earth and Planetary Science, The University of Tokyo, Tokyo, Japan*
[2]*National Institute of Polar Research, Tokyo, Japan*

We performed a campaign targeting atmospheric turbulence in the troposphere and lower stratosphere based on the PANSY radar observation using a frequency radar interferometric imaging (FII) technique during 14–24 March and 2–12 August 2019. In this campaign, 73 cases of Kelvin-Helmholtz (KH) billows were identified. KH billows in the upper troposphere and lower stratosphere were detected when the cyclone approached Syowa Station. We focused on two cases of the KH billows detected in the upper troposphere. Case A has the longest lifetime of all the cases. The KH billow was detected continuously for about 6.5 h on 21 March at z = 8.8 – 9.6 km. This case was likely caused by a strong vertical shear associated with orographic GWs over Syowa Station. On the other hand, Case B has the deepest vertical structure among all the cases. This KH billows was detected for about 2.0 h on 22 March at z = 6.2 – 7.8 km. It is likely that a southward jet in the upper troposphere associated with the cyclone caused shear instability. In addition, the stretched and elongated air mass with high temperature over Syowa Station provided thermal wind balance which strengthened the upper tropospheric jet.

Statistics for all 73 cases were also obtained in this study. Typical characteristics of KH billows in the Antarctic troposphere and lower stratosphere were demonstrated for the first time. These statistic show that the dynamical characterstics of KH billows in the Antarctic are consistent with those observed by the MU radar in the midlatitude, except for the period of billows and the strength of the vertical shear. In addition, a comparison between the linear instability theory and the observation was carried out. It is shown that the unstable mode with the maximum growth rate, which was calculated from the observed vertical profile of background winds and static stability, has similar characteristics to the observed KH billows.

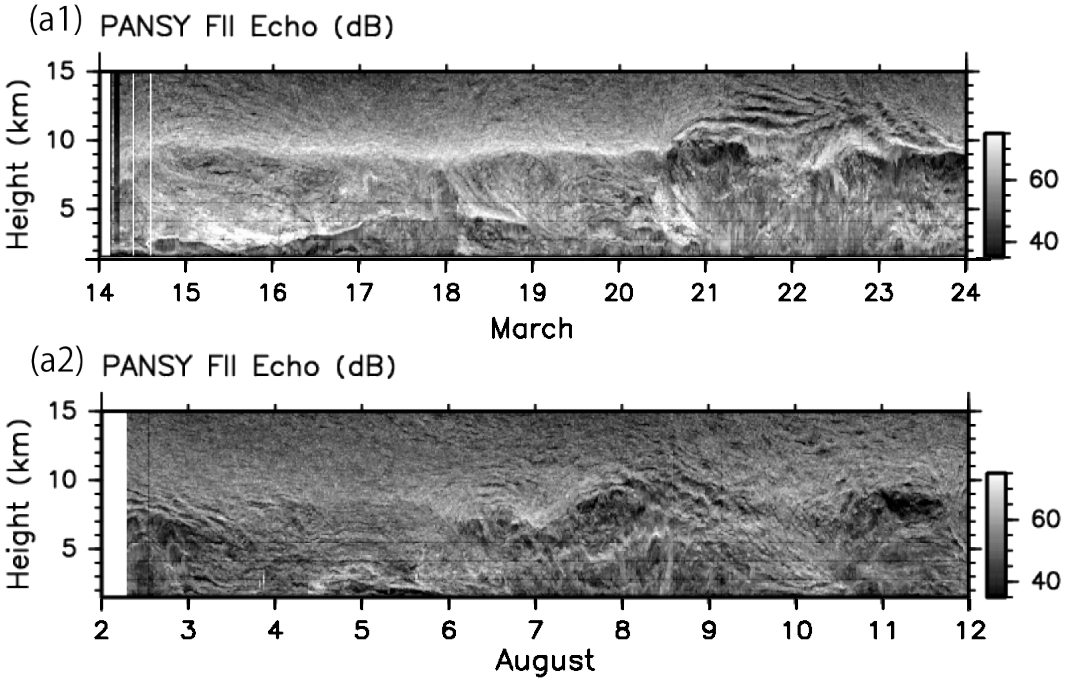

Figure 1: Time–height cross sections of scattering echo power observed by the FII mode of the PANSY radar for (a1) 14–24 March 2019 and (a2) 2–12 August 2019.

Characteristics and reproducibility of inertia gravity waves over Syowa Station ~Comparison between the PANSY radar and the ERA5 reanalysis~

Lihito Yoshida[1], Yoshihiro Tomikawa[2,1], Mitsumu K. Ejiri[2,1], Masashi Kohma[3] and Kaoru Sato[3]
[1] *School of Multidisciplinary Sciences, The Graduate University for Advanced Studies, SOKENDAI*
[2]*National Institute of Polar Research*
[3]*Graduate School of Science, The University of Tokyo*

Gravity waves (GWs) are atmospheric waves whose restoring force is buoyancy. They are originated mainly from mountains, jet-front systems, and convection, and can modify a global wind structure through momentum transport and deposit. They do not only decelerate the upper part of the mesospheric jets, but also affect the horizontal winds in the lower stratosphere, and contribute to drive the global meridional circulation. However, GW observations are usually not enough to verify their behaviour in the Antarctic, due to the harsh environment. In addition, GWs have a wide range of horizontal wavelength (i.e., from several km to several thousand km) and period (i.e., from Brunt-Väisälä period (approximately 5 minutes) to inertial period (over 12 hours), which makes it difficult to reproduce GWs in the entire frequency range even in the state-of-the-art atmospheric models in spite of the recent increase of the model resolution. In order to implement the effect of subgrid-scale phenomena into the models, which are not explicitly represented, GW parameterizations are introduced. In general, nonorographic GW parameterization assumes nearly constant wave sources and instantaneous upward propagation, but in reality the wave sources are not constant and GWs propagate horizontally as well (Sato et al., 2009; Geller et al., 2013; Plougonven et al., 2020). Thus it is required to constrain the GW effect in the models based on observations which cover the whole frequency range of GWs and estimate the GW momentum transport in the Antarctic.

Intermittency, a measure of how transient or intermittent a GW event is, has recently received much attention. Even if the total amount of momentum flux is the same, continuous, small amplitude events deposit momentum to higher altitudes, while sporadic and large amplitude events deposit momentum to lower altitudes. As a result, the structure and strength of the driven meridional circulation depend on the GW intermittency (Hertzog et al., 2008). In Antarctica, intermittency has been studied using super pressure balloons (Hertzog et al., 2012) and the Program of the Antarctic Syowa MST/IS radar (PANSY radar) at Syowa Station (Minamihara et al., 2020), suggesting differences in the characteristics of intermittency due to different wave generation mechanisms and wave filtering.

Our purpose of this study is to investigate the characteristics of GWs for sporadic and large amplitude events that can have a large impact on the overall momentum transport, and also to investigate how well the reanalysis data reproduces the GWs events in the Antarctic. We used the PANSY radar for the observation data and the ERA5 reanalysis for the reanalysis data. The PANSY radar, which was installed at Syowa Station (69°S,40°E) in 2011, observes vertical profiles of three dimensional winds in the troposphere and lower stratosphere with high accuracy and fine temporal and vertical resolution (Sato et al., 2014). It is the only instrument in the Antarctic that enables us to capture GWs in the almost entire frequency range. The ERA5 reanalysis is the latest meteorological reanalysis dataset provided by the European Centre for Medium-Range Weather Forecasts. The ERA5 data is distributed at 137 vertical levels from the surface to 0.01 hPa with a horizontal spacing of 0.25 degree every 1 hour.

We use three dimensional winds of the PANSY radar and the ERA5 reanalysis during the period of October 2015 to September 2016, in which the PANSY radar was continuously operated (Minamihara et. al.,2018). The inertia-GWs are extracted by applying a bandpass filter with a cutoff period of 4-24 h and a cutoff vertical wavelength of 0.8-8 km. As a result, we found many similar wave-like structures between the PANSY radar and the ERA5 reanalysis.

In order to examine the propagation characteristics of inertia-GWs, we use a hodograph analysis. It utilizes the feature that the hodograph (i.e., vertical change of the horizontal wind vector drawn in the zonal and meridional wind space) becomes an ellipse, in which the amplitude, intrinsic period, vertical wavelength, phase velocity, and group velocity of GWs can be estimated. Although the hodograph analysis generally has an ambiguity of horizontal propagation direction by 180°, we exclude it by comparing direct estimates of the ground-based wave period from the time altitude section.

We will discuss the similarities and differences between the PANSY radar and ERA5 reanalysis, as well as seasonal and altitude variations of sporadic GW events over Syowa Station.

References

Hertzog, A., Alexander, J. M., & Plougonven, R. (2012). On the intermittency of gravity wave momentum flux in the stratosphere. Journal of the Atmospheric Sciences, 69(11), 3433–3448. https://doi.org/10.1175/JAS-D-12-09.1

Sato, K., Tsutsumi, M., Sato, T., Nakamura, T., Saito, A., Tomikawa, Y., Nishimura, K., Kohma, M., Yamagishi, H., & Yamanouchi, T. (2014). Program of the Antarctic Syowa MST/IS radar (PANSY). Journal of Atmospheric and Solar-Terrestrial Physics, 118, 2–15. https://doi.org/10.1016/j.jastp.2013.08.022

Geller, M. A., Alexander, J. J., Love, P. T., Bacmeister, J., Ern, M., Hertzog, A., Manzini, E., Preusse, P., Sato, K., Scaife, A. A., & Zhou, T. (2013). A comparison between gravity wave momentum fluxes in observations and climate models. Journal of Climate, 26(17), 6383–6405. https://doi.org/10.1175/JCLI-D-12-00545.1

Plougonven, R., de la Cámara, A., Hertzog, A., & Lott, F. (2020). How does knowledge of atmospheric gravity waves guide their parameterizations? Quarterly Journal of the Royal Meteorological Society, 146(728), 1529–1543. https://doi.org/10.1002/qj.3732

Minamihara, Y., Sato, K., Tsutsumi, M., & Sato, T. (2018). Statistical Characteristics of Gravity Waves With Near-Inertial Frequencies in the Antarctic Troposphere and Lower Stratosphere Observed by the PANSY Radar. Journal of Geophysical Research: Atmospheres, 123(17), 8993–9010. https://doi.org/10.1029/2017JD028128

Minamihara, Y., Sato, K., & Tsutsumi, M. (2020). Intermittency of Gravity Waves in the Antarctic Troposphere and Lower Stratosphere Revealed by the PANSY Radar Observation. Journal of Geophysical Research: Atmospheres, 125(15). https://doi.org/10.1029/2020JD032543

Hertzog, A., Boccara, G., Vincent, R. A., Vial, F., & Cocquerez, P. (2008). Estimation of gravity wave momentum flux and phase speeds from quasi-Lagrangian stratospheric balloon flights. Part II: Results from the Vorcore campaign in Antarctica. Journal of the Atmospheric Sciences, 65(10), 3056–3070. https://doi.org/10.1175/2008JAS2710.1

Sato, K., Watanabe, S., Kawatani, Y., Tomikawa, Y., Miyazaki, K., & Takahashi, M. (2009). On the origins of mesospheric gravity waves. Geophysical Research Letters, 36(19), 1–5. https://doi.org/10.1029/2009GL039908

Contribution of gravity waves to the universal vertical wavenumber (m^{-3}) spectra revealed by a gravity-wave permitting general circulation model

Haruka Okui[1], Kaoru Sato[1] and Shingo Watanabe[2]
[1]*Department of Earth and Planetary Science, The University of Tokyo*
[2]*Japan Agency for Marine–Earth Science and Technology (JAMSTEC)*

Gravity waves (GWs) play fundamental roles in determining large-scale dynamical and thermal structure of the middle atmosphere by transporting momentum and energy. Based on radar and radiosonde observations, it has been known that power spectra versus vertical wavenumbers (m) of horizontal wind and temperature fluctuations have a common shape with a steep slope (e.g., VanZandt, 1982; Dewan & Good, 1986; Tsuda et al., 1989; Allen & Vincent, 1995). This common shape is approximately, but not necessarily, proportional to m^{-3} in a high wavenumber range. Applying the concept of GW saturation, several theories explaining the characteristic "m^{-3} spectra" have been developed (e.g., Smith et al., 1987; Sato & Yamada, 1994). However, it has not been fully confirmed that the observed m^{-3} spectra are really due to GWs.

To evaluate the contribution of gravity waves to the m^{-3} spectra, we used outputs from a hindcast of December 2018 using a GW-permitting general circulation model containing the surface to the lower thermosphere. GWs are extracted as fluctuations having total horizontal wavenumbers n= 21–639 (horizontal wavelengths of ~60–1900 km). In this study, we first verify the reproducibility of the observed spectral properties in the model. Next, the spectra of GWs are compared with those of fluctuations obtained from each single profile without horizontal wavenumber filtering. In addition, to examine the behavior of GWs in the middle atmosphere, parameters describing the characteristics of GW spectra are estimated.

Figures 1a–1f show the spectra in the lower stratosphere at z= 8–14 km and mesosphere at z= 68–88 km at Shigaraki (35°N, 136°E), Japan. The solid and dashed lines show the spectra of GWs and all fluctuations, respectively. The thin dotted lines represent the theoretical spectra proportional to m^{-3} proposed by Smith et al. (1987). These model-simulated spectra are in a good agreement with the theoretical spectra. This means that the model well reproduces the observed spectral property, that is, approximately proportional to m^{-3}.

The GW spectra are folded at a characteristic wavenumber (hereinafter m_{g*}) of 3–5×10^{-4} m^{-1} in the lower stratosphere and at 1–2×10^{-4} m^{-1} in the mesosphere. In the higher m range than m_{g*}, the GW spectra accord well with those of all fluctuations.

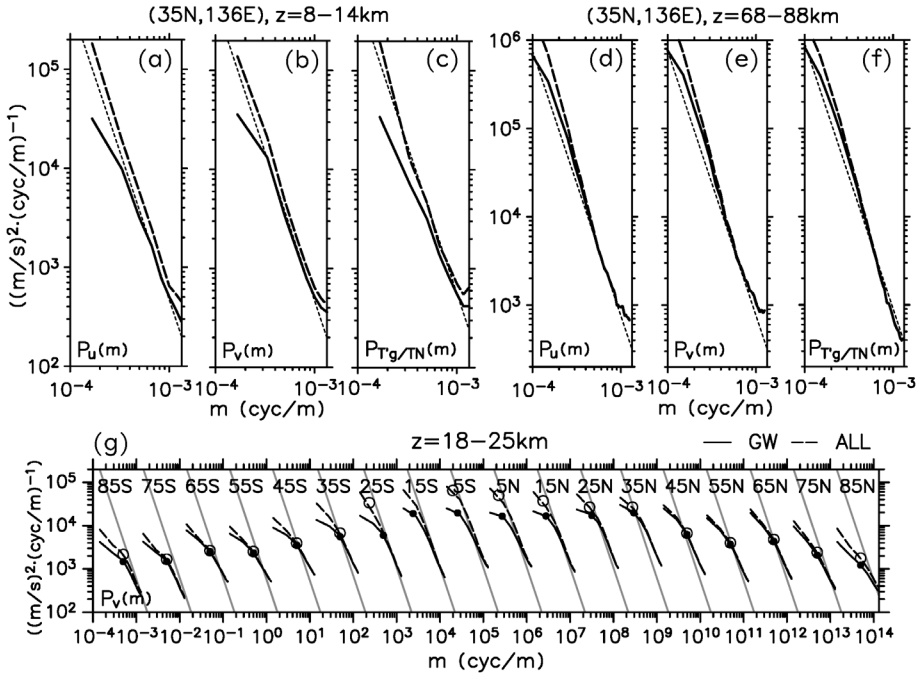

Figure 1. Vertical wavenumber spectra of (a, d) zonal wind, (b, e) meridional wind, and (c, f) temperature from 5–20 December 2018 at Shigaraki at (a-c) z= 8–14 and (d-f) 68–88 km. Solid and dashed curves show the spectra of GWs and all fluctuations, respectively. The theoretical spectra by Smith et al. (1987) are indicated by thin dotted lines. (g) Meridional wind spectra at z=18–25 km averaged zonally and over a latitude region of ±5°. Filled and open circles show the folding points of GW and all-fluctuation spectra, respectively. Gray lines are the theoretical spectra. The scale of the horizontal axis is for the spectra at 85°S and the other curves are shifted by an order of magnitude one by one.

On the other hand, for $m < m_{g*}$, the GW spectra are smaller even in the m^{-3} range of the spectra for all fluctuations. These facts suggest that fluctuations other than the GWs also considerably contribute to the spectra at lower m in the m^{-3} range. The folding wavenumber m_{g*} is lower in the mesosphere than in the lower stratosphere. This difference between the two height regions shows that GWs are dominant even at lower m in the mesosphere. Figure 1g shows the spectra at z= 18–25 km averaged zonally and over a latitudinal range of ±5° around respective latitudes. The disagreement between the spectra for GWs and those for all fluctuations is large especially in the equatorial region. In this region, characteristic wavenumbers of the all-fluctuation spectra (denoted by open circles) are lower than those of the GW spectra (filled circles). It is likely that these disagreements of the spectra are due to the contribution of equatorial waves.

By fitting obtained GW spectra to the following equation (Allen & Vincent, 1995):

$$P(m) = F_0 \frac{m/m_{g*}}{1 + \left(m/m_{g*}\right)^{t+1}}$$

parameters m_{g*}, t and F_0 are estimated. The parameters t and F_0 represent the spectral slope of opposite sign and the amplitude at m_{g*}, respectively. Figure 2 shows the latitudinal distributions of these parameters for the spectra of GW meridional wind fluctuations. At most latitudes, the characteristic wavenumber m_{g*} is lower at higher altitudes (Fig. 2a). The parameter F_0 is larger at higher altitudes (Fig. 2c). These characteristics are attributable to the wave amplification due to the exponential decrease in density and to the wave saturation at high m. At mid- and high latitudes, t increases with altitude. It is inferred that, in addition to the wave saturation, strong vertical wind shear below the winter and summer jets contributes to the increase in t at mid- and high latitudes.

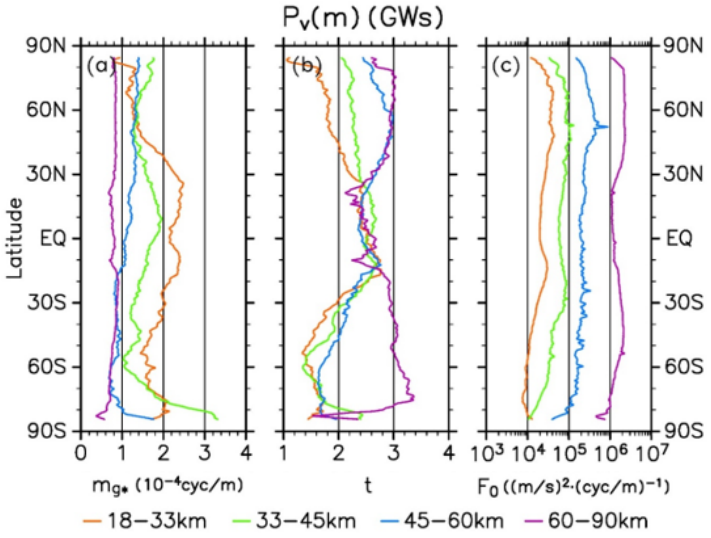

Figure 2. Latitudinal distributions of the zonal mean (a) m_{g*}, (b) t and (c) F_0 for meridional wind spectra of GWs from 5–20 December 2018. The colors of the curves represent respective altitude regions shown at the bottom of the figure.

References

Allen, S. J., & Vincent, A. (1995). Gravity wave activity in the lower atmosphere: Seasonal and latitudinal variations. *Journal of Geophysical Research*, **100**, 1327– 1350. https://doi.org/10.1029/94JD02688

Dewan, E. M., & Good, R. E. (1986). Saturation and the "universal" spectrum for vertical profiles of horizontal scalar winds in the atmosphere. *Journal of Geophysical Research*, **91**(D2), 2742–2748. https://doi.org/10.1029/JD091iD02p02742

Sato, K., & Yamada, M. (1994). Vertical structure of atmospheric gravity waves revealed by the wavelet analysis. *Journal of Geophysical Research*, **99**(D10), 20,623–20,631. https://doi.org/10.1029/94JD01818

Smith, S. A., Fritts, D. C., & Vanzandt, T. E. (1987). Evidence for a Saturated Spectrum of Atmospheric Gravity Waves, *Journal of Atmospheric Sciences*, **44**(10), 1404–1410. https://doi.org/10.1175/1520-0469(1987)044%3C1404:EFASSO%3E2.0.CO;2

Tsuda, T., Inoue, T., Kato, S., Fukao, S., Fritts, D. C., & VanZandt, T. E. (1989). MST Radar Observations of a Saturated Gravity Wave Spectrum, *Journal of Atmospheric Sciences*, **46**(15), 2440–2447. https://doi.org/10.1175/1520-0469(1989)046%3C2440:MROOAS%3E2.0.CO;2

VanZandt, T. E. (1982). A universal spectrum of buoyancy waves in the atmosphere. *Geophysical Research Letters*, **9**, 575–578. https://doi.org/10.1029/GL009i005p00575

Gravity Wave Weakening in the 2019 Antarctic Stratospheric Sudden Warming

Masaru Kogure[1], Jia Yue[2,3] and Huixin Liu[1]
[1] *Department of Earth and Planetary Science, Kyushu University, Fukuoka, Japan*
[2]*NASA Goddard Space Flight Center, Greenbelt, MD, USA*
[3]*Physics Department, Catholic University of America, Washington, DC, USA*

A rare Antarctic stratospheric sudden warming (SSW) occurred on late August, 2019, and was a minor warming event. This study investigated variations in gravity wave (GW) activity before and after this Antarctic SSW event using AIRS and CIPS (two satellite measurements) and GEOS-5 FP (reanalysis data). GW activity over the Andes decreased after the SSW onset, although the westerly wind was 40–60 ms^{-1} and cannot filter out GWs with small zonal phase speed. This decline over the Andes was probably caused by wave saturation. Zonal mean GW activity over the Antarctic and the Southern Ocean likewise decreased, with a weakening of zonal wind. The zonal mean GW activity further decreased around early September which coincided with a reversal of the zonal mean zonal wind at 40 km. The decline in the zonal mean GW activity after the onset was probably caused by wind filtering and polar night jet breaking.

References

Kogure, M., Yue, J., & Liu, H. (2021). Gravity wave weakening during the 2019 Antarctic stratospheric sudden warming. Geophysical Research Letters, 48, e2021GL092537.

An event study on sporadic Fe layer at Syowa station (69.0°S, 39.6°E) based on numerical simulation and simultaneous observation of Fe density and wind

T. Nishiyama[1,2], M. K. Ejiri[1,2], T. T. Tsuda[3], K. Tsuno[4], T. Nakamura[1,2], M. Tsutsumi[1,2],
M. Abo[5], T. D. Kawahara[6], T. Ogawa[4], and S. Wada[4]
[1]*National Institute of Polar Research, Japan*
[2]*Department of Polar Science, The Graduate University for Advanced Studies, SOKENDAI, Japan*
[3]*The University of Electro- Communications*
[4]*ASI, RIKEN*
[5]*Tokyo Metropolitan University.*
[6]*Faculty of Engineering, Shinshu University.*

Mesospheric metal layer which are formed by atoms ablated from moteoroids are known to be between 80 and 105 km in the terrestrial atmosphere. Meteoric species such as Fe, Mg, and Na exist as atoms in the layers and their dynamical and chemical variability have been investigated by resonance scattering lidars [Plane et al., 2015 and references therein] and satellite-borne measurements. Sporadic E layer, Es layer, is characterized as a thin layer with enhanced electron density and mainly observed by incoherent scatter radars and ionosondes. Mg^+ and Fe^+ ions are regarded as dominant ion components in Es layers due to their long lifetime, and therefore sporadic metallic layers are believed to play important roles in forming Es layers. Suggested generation mechanisms of sporadic metallic layers in polar regions are mainly as follows: vertical ion converge and neutralization due to wind shear [e.g., Nygrén et al., 1984] and ionospheric electric field [e.g., Kirkwood and von Zahn, 1991].

We identified sporadic Fe, hereafter FeS, event on June 5, 2018 at Syowa station (69.0°S, 39.6°E), Antarctic, that was observed by a resonance scattering lidar. This FeS event can be summarized as follows: a center altitude and FWHM of the FeS layer are 90 km and 5 km, respectively, duration about 3 hours, quiet geomagnetic activity during this event, intermittent Es activity identified by co-located ionosonde, and quite slow apparent growth rate of 1.5 %/min for the FeS. During the FeS event, neutral wind data from an MF radar at Syowa is available. We have tried to explain the observed FeS by wind shear theory. Ion-neutral collision frequency for Fe^+ was estimated by an empirical model of Voiculescu and Ignat [2002], NRLMSISE-00, and IGRF-13. In addition, vertical Fe^+ ion velocity and its temporal variations were calculated in consideration of magnetic declination [Yu et al., 2019]. These imply that Fe^+ converge took place earlier than FeS peak (about 8 hours). Fe^+ neutralization with a time scale of about a few hours is consistent with the observed FeS.
We ran numerical simulations including Fe/Fe^+ chemistry and 1-D vertical transportation of Fe^+ using the estimated ion vertical velocity. Initial density profiles of Fe/Fe^+ and related species are based on model results of *Feng et al.* [2013]. The simulation result shows that weak FeS was reproduced at 93 km, but peak Fe density was only half of the observation. Next, we used another Fe^+ ion velocity profile, which is a few times larger below 100 km altitude for additional running as a numerical experiment. As a result, strong FeS was successfully reproduced at 94 km with almost the same growth rate as the observations. These results suggest that we still underestimated Fe^+ ion velocity, especially below 100 km. We should take account into the following in near future: neutral Fe vertical transportation, horizontal advection, and three-dimensional wind with larger amplitudes in small spatial scale.

References

J. M. C. Plane, W. Feng, and E. C. M. Dawkins, The Mesosphere and Metals: Chemistry and Changes, Chem. Rev., 115(10), 4497–4541, 2015.
T. Nygrén, L. Jalonen, J. Oksman, and T. Turunen, The role of electric field and neutral wind direction in the formation of sporadic E-layers, Journal of Atmospheric and Terrestrial Physics, 46(4), 373 – 381, 1984.
S. Kirkwood, and U. von Zahn, On the role of auroral electric fields in the formation of low altitude sporadic-E and sudden sodium layers, Journal of Atmospheric and Terrestrial Physics, 53(5), 389 – 407, 1991.
M. Voiculescu1 and M. Ignat, Vertical motion of ionization induced by the linear interaction of tides with planetary waves, Annales Geophysicae, 21, 1521–1529, 2003
B. Yu, X. Xue, X. Yue, C. Yang, C. Yu, X. Dou, B. Ning, and L. Hu, The global climatology of the intensity of the ionospheric sporadic E layer, Atmos. Chem. Phys., 19, 4139–4151, 2019
Feng, W., D. R. Marsh, M. P. Chipperfield, D. Janches, J. Höffner, F. Yi, and J. M. C. Plane (2013), A global atmospheric model of meteoric iron, J. Geophys. Res. Atmos., 118, 9456–9474, doi:10.1002/jgrd.50708.

An advanced meteor wind study based on MF radar observations over Syowa (69S,39E), Antarctic

Masaki Tsutsumi[1], Taishi Hashimoto[1], Koji Nishimura[2], Toru Sato[3], Masashi Kohma[4] ,and Kaoru Sato[4]
[1]*National Institute of Polar Research*
[2]*RISH, Kyoto Univ,* [3]*ILAS, Kyoto Univ.,* [4]*Graduate School of Science, Univ. of Tokyo*

MF (Middle Frequency) radars have been used to measure wind velocity in mesosphere and lower thermosphere based on correlation analysis techniques [e.g., Reid, 2015]. The techniques assume that weakly ionized atmosphere is usually horizontally stratified, and that radar echoes from such layered atmosphere are mostly obtained in the vertical direction. However, there also exist MF radar echoes coming back from large off-vertical angles. Meteor echoes are such type of echoes often detected at night (winter time in the polar region) mostly above 80 km. Because of the low radio frequency (2-3 MHz) the duration of MF radar meteor echoes is two orders longer than that of VHF meteor echoes. Thus, meteor echoes can sometimes dominate the MF radar echoes when the background atmospheric ionization is relatively low. These meteor echoes have been used to compensate the known problem of MF radar correlation technique above about 90 km [Tsutsumi and Aso, 2005].

We have recently scrutinized the MF radar meteor measurement technique being conducted at Syowa station (59S, 39E), Antarctica, and found that wind velocity can be estimated with a time resolution as good as 10 min under preferable ionospheric conditions. Such resolution is remarkably high as meteor wind measurements. Horizontal structure of wind field can be further estimated within the horizontal region of 200 x200 km (see Figure 1). Estimation of momentum flux deposition may be possible using the method proposed by Hocking [2005]. The obtained results are to be verified by comparing with those observed by the co-locating MST/IS radar (PANSY radar) [Sato et al, 2014].

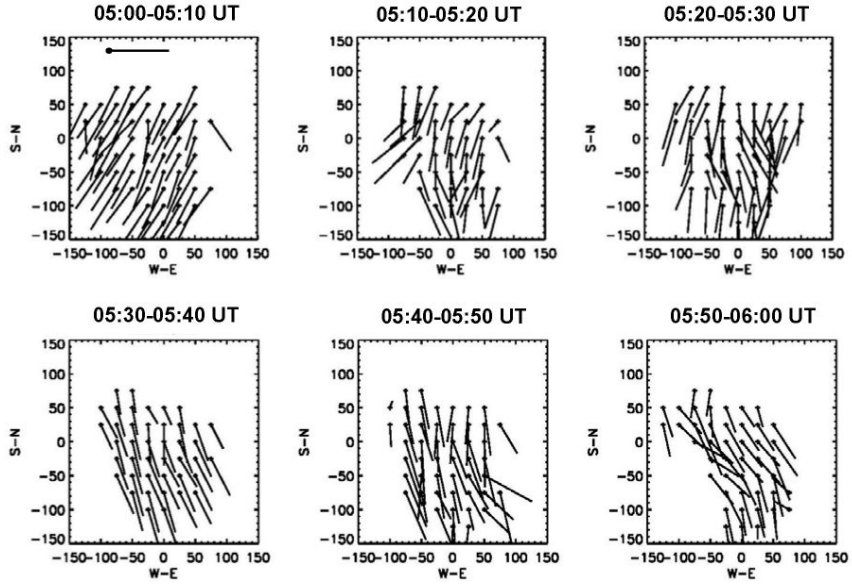

Figure 1: Two-dimensional structures of horizontal wind velocity at 88 km altitude observed on May 1, 2018, over Syowa station (69S, 39E), Antarctic. The horizontal region of 300 x 300 km is shown. Each wind vector is estimated using echoes detected within the corresponding sub-region with horizontal dimensions of 50 x 50 km.

References

Hocking, W. K., A new approach to momentum flux determinations using SKiYMET meteor radars, *ANGEO* 23(7):2433–9, http://dx.doi.org/10.5194/angeo-23-2433-2005, 2005.

Reid, I. M., MF and HF radar techniques for investigating the dynamics and structure of the 50 to 110 km height region: A review., *Prog. in Earth and Planet. Sci.*, 2, doi:10.1186/s40645-015-0060-7, 2015.

Sato, K., M. Tsutsumi, T. Sato, T. Nakamura, A. Saito, Y. Tomikawa, K. Nishimura, M. Kohma, H. Yamagishi, T. Yamanouchi, Program of the Antarctic Syowa MST/IS radar (PANSY), *J. Atmos. Sol-Terr. Phys.*, 118, 2-15, 2014.

Tsutsumi, M., and T. Aso, MF radar observations of meteors and meteor-derived winds at Syowa (69 degrees S, 39 degrees E), Antarctica: A comparison with simultaneous spaced antenna winds , *J. Geophys. Res -Atmos.*, 110, doi:10.1029/2005JD005849 2005.

High altitude meteors detected by the interferometric MU radar

Daniel Kastinen[1,2] and Johan Kero[1]
[1]*Swedish Institute of Space Physics (IRF), Box 812, SE-98128 Kiruna, Sweden*
[2]*Umeå University, Department of Physics, SE-90187 Umeå, Sweden*

During the last few years, we have been engaged in an effort to significantly update the meteor head echo analysis pipeline used at the MU radar in Shigaraki, Japan. Now at the end of this process, as a direct application of the improvements, we re-analysed the MU radar meteor head echo data set collected during 2009-2010. In this dataset we have now confirmed the existence of a rare high-altitude radar meteor population with starting ablation altitudes reaching up to ~150 km. The number of detections decrease significantly as a function of initial altitude. Out of the total amount of 106,000 events, 74 had an initial altitude >130 km while 4 of those had an initial altitude >145 km.
High-altitude radar meteor observations have been reported before, e.g. using the EISCAT VHF radar (monostatic dish) and the Jicamarca Radio Observatory (4 channel interferometry). The novelty of our results is that the observations were performed and analysed in such a way that the meteor altitude is unambiguous. The MU radar used 25 channel interferometry where 6 of the antenna subgroups had asymmetric shape and baselines. The new pipeline was also rigorously tested by noisy raw data simulations to show its unambiguous DOA determination capabilities (Kastinen & Kero, 2020). However, due to the experimental setup used during the 2009-2010 campaigns the maximum detectable range was limited to 148 km. Hence, we cannot confirm or deny the existence of radar meteors above that altitude.

The previous pipeline used at the MU radar is described in detail in (Kero, et al., 2012). The new pipeline has three major differences from the previous: improved basic algorithms, noisy raw data simulation to validate and predict measurement error distributions, and Markov Chain Monte Carlo (MCMC) trajectory fitting routines to derive probability distributions over model parameters. The improved basic algorithms included allowing the radar pulse decoding (i.e., matched filtering) to handle analysis of partial codes. This allowed the new pipeline to analyse events up to the maximum detection range of 148 km. The uncertainty estimations allowed these high-altitude detections to be validated. As additional validation all remaining events were parsed manually.

The existence and characteristics of high-altitude radar meteors alludes to information on the material and composition properties of the meteoroids in question. Ordinary thermal ablation modeling does not predict the high-altitude meteor population (Popova, et.al, 2019). Therefore, either the composition or material is different in the high-altitude population or the ablation physics are different. Both avenues are of interest to atmospheric science as they influence the distribution, both composition and altitude, of extraterrestrial input of material into the atmosphere. Material that affects various physical and chemical processes and a wide range of phenomena, such as the formation of clouds at 15-25 km altitude responsible for ozone destruction in the polar regions, mid-latitude ice clouds at 75-85 km which are possible tracers of global climate change, and metallic ion layers in the atmosphere (Plane, 2003).

References

Kastinen, Daniel, and Johan Kero. "Probabilistic analysis of ambiguities in radar echo direction of arrival from meteors." *Atmospheric Measurement Techniques* 13.12 (2020): 6813-6835.
Kero, Johan, et al. "A meteor head echo analysis algorithm for the lower VHF band." *Annales Geophysicae*. Vol. 30. No. 4. Copernicus GmbH, 2012.
Popova, Olga, Jirí Borovicka, and M. Campbell-Brown. "Modelling the entry of meteoroids." Meteoroids: Sources of Meteors on Earth and Beyond 25 (2019): 9.
Plane, John MC. "Atmospheric chemistry of meteoric metals." Chemical reviews 103.12 (2003): 4963-4984.

Developing the NASA Atmospheric Waves Experiment (AWE)

M. J. Taylor[1], J. M Forbes[2], D. C. Fritts[3], J. B. Snively[4], S. D. Eckermann[5], H.-L. Liu[6], P.-D. Pautet[1], Y. Zhao[1], E. Syrstad[7], R. Esplin[7], B. Lamborn[7], H. Latvakoski[7]

[1]*Utah State University, Logan, Utah, USA*

[2]*University of Colorado, Boulder, Colorado, USA*

[3]*GATS, Boulder, Colorado, USA*

[4]*Embry Riddle Aeronautical University, Daytona Beach, Florida, USA*

[5]*Naval Research Laboratory, Washington, District of Columbia, USA*

[6]*National Center for Atmospheric Research, High Altitude Observatory, Boulder, Colorado, USA*

[7]*Utah State University, Space Dynamic Laboratory, Logan, Utah, USA*

The Atmospheric Waves Experiment (AWE) is a NASA Heliophysics Explorers Mission of Opportunity (MO) Program designed specifically to investigate the near-global properties and effects of gravity waves (GW) as they propagate into the Earth's upper atmosphere. In particular, AWE will measure the spectrum of small-scale (~30-300 km) GWs generated by strong weather disturbances, such as deep convection and sustained flow over mountains, that impact the Ionosphere, Thermosphere and Mesosphere (ITM).

The AWE instrument is currently under development at the Space Dynamics Laboratory (SDL) at Utah State University (USU) and comprises a novel, wide-field of view (~600 km), 4-channel infrared imaging system. It is based on the successful USU ground-based Advanced Mesospheric Temperature Mapper (AMTM) which measures selected emission lines in the OH (3,1) band to image GW in the OH airglow layer (~87 km) and at the same time to estimate atmospheric temperatures using the well-established "ratio method". The completed AWE flight instrument is currently scheduled to be deployed on the International Space Station (ISS) in July, 2023.

The ISS provides a near-ideal combination of geographic and local-time coverage to accomplish our proposed GW science, which seeks not only near-global measurements (85% coverage) of wave spectral characteristics and correlations with their copious sources, but also quantifications of GW amplitudes, variances, and fluxes of momentum and energy into the ITM. Two years of nadir viewing GW measurements are planned. Combined with state-of-the-art general circulation and high-resolution regional models the AWE mission will quantify the relative importance of source inputs versus propagation conditions towards determining effects of GW on the ITM. The first data products will be made available to the scientific community within 6 months of launch with planned long-term data archiving at the NASA Space Physics Data Facility (SPDF). We welcome your interests in this exciting mission.

Airglow observations from International Space Station by ISS-IMAP/VISI

A. Saito[1], T. Sakanoi[2] , Y. Hozumi[3], , S. Perwitasari[3] and ISS-IMAP working group
[1]*Graduate School of Science, Kyoto University, JAPAN*
[2]*Graduate School of Science, Tohoku University, JAPAN*
[3]*National Institute of Information and Communications Technology, JAPAN*

ISS-IMAP (Ionosphere, Mesosphere, upper Atmosphere, and Plasmasphere mapping) mission consisted of two imagers, Visible-light and infrared spectrum imager (VISI) and Extra ultraviolet imager (EUVI), and observed the Mesosphere, Thermosphere and Ionosphere (MTI) region from the Exposed Facility of Japanese Experiment Module of the International Space Station between 2012 and 2015. VISI observed emissions of airglow and aurora of 730nm (OH, Alt. 85km), 762nm (O2, Alt. 95km), and 630nm (O, Alt. 250km) [Sakanoi et al., 2011], and Extra ultraviolet imager (EUVI) observed the resonant scattering of 30.4nm (He+) and 83.4nm (O+) from ion in the Ionosphere and Plasmasphere [Yoshikawa et al., 2011, Nakano et al., 2021]. VISI's observations of airglow at 762 nm, with its wide coverage and high spatial resolution, have revealed several new features of the Mesosphere. One of them is the distribution of the concentric wave structures that are generated by atmospheric gravity waves propagating from the lower atmosphere with spatially limited sources [Perwitasari et al., 2015; 2016]. They were frequently observed around 40 degrees of the geographic latitudes in the both hemispheres. Some of them were interpreted to be attributed to the tropospheric phenomena, such as tornados and typhoons considering coincidence of space and time [Akiya et al., 2014]. Another phenomenon that was revealed its global distribution is the mesospheric bores [Hozumi et al., 2018; 2019]. More than 300 events of the mesospheric bores were identified by the VISI airglow observation, and it was found that they have high occurrence during equinox at low latitudes and during winter at mid-latitudes. For the ionospheric phenomena, the occurrence distribution of plasma bubbles on the bottom side of the ionospheric F-region is investigated with the airglow at 630nm [Nakata et al., 2018]. Coupling processes form the lower atmosphere to the upper atmospheres that have been revealed by the ISS-IMAP/VISI observation will be discussed in the presentation.

References

Akiya, Y., A. Saito, T. Sakanoi, Y. Hozumi, A. Yamazaki, Y. Otsuka, M. Nishioka, and T. Tsugawa, First space-borne observation of the entire concentric airglow structure caused by tropospheric disturbance, Geophysical Research Letters, 41, 6943-6948, doi: 10.1002/2014GL061403, 2014.

Hozumi, Y., Saito, A., Sakanoi, T., Yamazaki, A., and Hosokawa, K., Mesospheric bores at southern midlatitudes observed by ISS-IMAP/VISI: a first report of an undulating wave front, Atmos. Chem. Phys. Discuss., doi:10.5194/acp-2018-383, 2018.

Hozumi, Y., A. Saito, T. Sakanoi, A. Yamazaki, K. Hosokawa, and T. Nakamura, Geographical and seasonal variability of mesospheric bores observed from the International Space Station, J. Geophys. Res. Space Physics, 124,3775–3785, doi:10.1029/2019JA026635, 2019.

Nakano, S., Hozumi, Y., Saito, A., Yoshikawa, I., Yamazaki, A., Yoshioka, K. and Murakami, G., EUV signals associated with O+ ions observed from ISS-IMAP/EUVI in the nightside ionosphere, Earth, Planets and Space, 73, 151, https://doi.org/10.1186/s40623-021-01479-0, 2021.

Nakata, H., A. Takahashi, T. Takano, A. Saito and T. Sakanoi, Observation of equatorial plasma bubbles by the airglow imager on ISS-IMAP, Progress in Earth and Planetary Science, 5, 66-78, doi:10.1186/s40645-018-0227-0, 2018.

Perwitasari, S., T. Sakanoi, A. Yamazaki, Y. Otsuka, Y. Hozumi, Y. Akiya, A. Saito, K. Shiokawa, S. Kawamura , Coordinated airglow observations between IMAP/VISI and a ground-based all-sky imager on concentric gravity wave in the lower thermosphere, J. Geophysical Research, doi: 10.1002/2015JA021424, 2015.

Perwitasari, S., T. Sakanoi, T. Nakamura, M. K. Ejiri, M. Tsutsumi, Y. Tomikawa, Y. Otsuka, A. Yamazaki, and A. Saito, Three years of concentric gravity wave variability in the mesopause as observed by IMAP/VISI, Geophys. Res. Lett., 43, 11,528–11,535, doi:10.1002/2016GL071511, 2016.

Sakanoi, T., Y. Akiya, A. Yamazaki, Y. Otsuka, A. Saito, I. Yoshikawa, Imaging observation of the earth's mesosphere, thermosphere and ionosphere by VISI of ISS-IMAP on the international space station, IEEJ Trans. on Fundamentals and Materials, vol. 131, 12, 983-988, doi: 10.1541/ieejfms.131.983, 2011.

Yoshikawa, I., T. Homma, K. Sakai, G. Murakami, K. Yoshioka, A. Yamazaki, T. Sakanoi and A. Saito, Imaging Observation of the Earth's Plasmasphere and Ionosphere by EUVI of ISS-IMAP on the International Space Station, IEEJ Trans. on Fundamentals and Materials, vol. 131, 12, 1006-1010, doi: 10.1541/ieejfms.131.1006, 2011.

Characteristics of gravity wave horizontal phase velocity spectra in the mesosphere over the Antarctic stations, Syowa and Davis.

Masaru Kogure[1], Takuji Nakamura[2,3], Damian J. Murphy[4], Michael J. Taylor[5], Yucheng Zhao[5], Pierre-Dominique Pautet[5], Masaki Tsutsumi[2,3], Yoshihiro Tomikawa[2,3], Mitsumu K. Ejiri[2,3], Takanori Nishiyama[2,3]
[1]Department of Earth and Planetary Science, Kyushu University, Fukuoka, Japan.
[2]National Institute of Polar Research.
[3]Department of Polar Science, SOKENDAI (The Graduate University for Advanced Studies), Tachikawa, Japan.
[4]Australian Antarctic Division, Department of Agriculture, Water and the Environment, Kingston, Australia.
[5]Center for Atmospheric and Space Sciences/Physics Department, Utah State University, Logan, UT, USA.

Mesospheric gravity-wave (GW) phase velocity spectra and total powers at two Antarctic stations, Davis and Syowa, were derived using OH airglow image data from March to October in 2016. The total powers have similar seasonal variation, that is, maxima in winter at both stations. However, the power at Davis was one standard deviation larger in winter and three times smaller in September than at Syowa. The total power at Davis in winter was mainly attributed to GWs with high eastward (≥ ~50 ms^{-1}) phase velocity. On the other hand, the higher total power at Syowa in September was attributed to GWs with omnidirectional phase velocity. These differences between Syowa and Davis cannot be explained by the wind filtering effect, and other factors are needed. To further explorer the origin of the difference in winter, we focused on an event on August 29, 2016, in which GWs with ~100 ms^{-1} southeastward phase velocity appeared at Davis. The raytracing method was applied, and its result indicated that those GWs with high southeastward phase velocity propagated from ~45 km altitude over the southern ocean (~43°E, ~58°S) where GWs with high amplitude and southeastward propagating emitted from the tropospheric jet appeared. These jet GWs were probably saturated in 45-50 km altitudes. Therefore, the GWs with eastward phase velocity were probably secondary gravity waves. This result suggests that the higher power in the eastward high phase velocity domain at Davis was contributed to by secondary GWs.

References

Kogure, M., Nakamura, T., Murphy, D., Taylor, M. J., Zhao, Y., Pautet, P. D., Tsutsumi, M., Tomikawa, Y., Ejiri, K. M., Nishiyama, T., Characteristics of gravity wave horizontal phase velocity spectra in the mesosphere over the Antarctic stations, Syowa and Davis, ESSOAr, doi:10.1002/essoar.10508064.1, 2021.(プレプリント, 査読中, submitted to JGR:Atmospheres)

Propagation direction analysis of medium-scale traveling ionospheric disturbances (MSTIDs) observed with 2D GPS-TEC map using three-dimensional spectral analysis method over North America

Septi Perwitasari[1], Takuji Nakamura[2,3], Takuya Tsugawa[1], Michi Nishioka[1], Yoshihiro Tomikawa[2,3], Mitsumu K. Ejiri[2,3], Masaru Kogure[4], Yuichi Otsuka[5], Atsuki Shinbori[5], Hidekatsu Jin[1] and Chihiro Tao[1]

[1]*National Institute of Information and Communications Technology (NICT)*

[2]*National Institute of Polar Research (NIPR)*

[3]*The Graduate University for Advance Studies, SOKENDAI*

[4]*Department of Earth and Planetary Sciences, Kyushu University*

[5]*ISEE, Nagoya University*

We applied a novel three-dimensional spectral analysis method to GPS-TEC maps over North America to study the propagation direction of daytime and nighttime MSTIDs. This method automatically calculates the phase velocity spectrum and directionality of MSTIDs. We focused on the period of high MSTIDs occurrence, June-July 2006 for nighttime and November-December 2006, to study daytime MSTIDs. We divided North America into the west (100°-130°W, 25°-55°N) and east (70°-100°W, 25°-55°N) part. Our results show that MSTIDs propagations exhibit strong longitudinal variation as a function of local time and daily variation for both daytime and nighttime MSTIDs. The daytime local time variation demonstrates that the MSTIDs rotate clockwise with the power peaks between 10:00-16:00 LT (10:00-14:00 LT) in the west part, however similar rotation is not very pronounced in the east part. The dominant propagation direction of daytime MSTIDs is southward (southeastward) in the west (east), respectively. The wind filtering is likely responsible for the longitudinal and local time variation of daytime MSTIDs. The local time variation of nighttime MSTIDs shows the power peaks between 22:00-02:00 LT (20:00-00:00 LT) in the west (east). We found the dominant propagation direction in the west part shifts westward with a wider azimuthal band (~210°-300°) than the east part (~210°-250°). Comparing nighttime MSTIDs propagation directions between western and eastern sides leads to a conclusion that magnetic declination angle has some influence.

Multi-wavelength auroral imaging observation with attitude-stabilized all-sky imagers on Shirase

Takeshi Sakanoi[1], Saki Yamashina[2], Yuta Hozumi[3], Takuo T. Tsuda[4], Takeshi Aoki[4], Takahiro Naoi[3]
Masato Nagahara[3], Akinori Saito[2], Mitsumu K. Ejiri[5], Takanori Nishiyama[5]
[1]*Planetary Plasma and Atmospheric Research Center, Graduate School of Science, Tohoku University*
[2]*Kyoto University*, [3]*NICT*, [4]*The University of Electro-Communications*, [4]*NICT*, [5]*NIPR*

We report the results of data analysis obtained with attitude-stabilized multi-wavelength all-sky imagers on Shirase during the period of JARE 61 (2019-2020) and 62 (2020-2021), and the current status of this project in JARE 63 (2021-2022). The purpose of this study is to observe aurora and airglow emission in the the Southern Ocean since ground-based imagers do not cover the ocean area. The nominal route of Shirase from February to March is located in the south of Australia which is suitable to observe aurora, and also important region to understand the height and zonal variations of mesospheric atmospheric gravity waves (AGWs). Our all-sky image data on Shirase is useful for collaboration with ground-based imager network, such as ANGWINS, UAO and AGO. In addition to the high-latitude observation, we expect to detect plasma bubbles and MSTID when Shirase is located at the mid- and low-latitudes between Japan and Antarctica.

In 2019, we developed a monochromatic all-sky imager at 630 nm, and succeeded to carry out continuous observation on Shirase during the period of JARE 61. In 2020, we developed another all-sky imager which covers 650-690 nm emission for N2 aurora and OH airglow. Furthermore, a GNSS receiver was installed in 2020 to monitor ionospheric total electron content. Each all-sky imager consists of a low-noise commercial CMOS camera (ZWO ASI183MM Pro), fisheye lens (Fujinon FE185C086HA, f=2.7 mm, F/1.8) and bandpass filter made of Andover. The sensitivity of two imagers were calibrated by the integrated sphere in NIPR in 2019 and 2021, and we confirmed that each imager has sufficient dynamic range (80 - 20000 R) and resolution (~5 R) with an exposure time of 19s. Two imagers were mounted on a 3-axis attitude stabilized gimbal (DJI Ronin-S), and installed in the water-proof observation box installed on the 06 deck of Shirase. We confirmed the performance of attitude stabilization by the gimbal of which vibration was attenuated by 1/14, and the spatial resolution of obtained image was sufficient for auroral and airglow observation. The controlling PC was installed in the observation room of Shirase, and routinely calculate appropriate start and end observation timings using GPS data, and operates all-sky imagers every day. Exposure and interval times were set to be 19 s and 20 s for the period of JARE 61 in 2019-2020, and 9 s and 10s for JARE 62 in 2020-2021. All data were stored in RAID hard disk system, and used for detailed analysis after Shirase's return to Japan in Spring in each year. During the cruise, thumbnail images and housekeeping data were sent to Japan via e-mail everyday to monitor the status. The temperature in observation box was controlled by heater and cooler throughout the operation period.

For the JARE 61 period, we succeeded to carry out automatic and continuous observations for 4 months throughout the cruise of Shirase. On several nights from February to March in 2020, we observed 630nm auroral emission with intensity of several kR in the northward direction when Shirase existed in the polar cap region. For the period of JARE 62 in 2020-2021, due to the COVID-19 situation Shirase went directly back and forth between Japan and Syowa. Therefore, we could not obtain auroral data because dark night conditions were not satisfied at high-latitudes. However, we obtained the data at mid- to low-latitudes on 10 nights out of total 48 nights with clear sky or partial clear sky conditions.

In 2021, as a part of JARE 63, we changed the gimbal to Ronin-RS2, and improved the control system. We also changed the filter bandwidth of the imager for N2 aurora and OH airglow to cover the wavelength in the near-infrared range from 720 to 800 nm where OH airglow is more intense. The improved system was installed on Shirase in August 2021, and automatic and continuous operation has been started. The departure of Shirase is scheduled in the middle of November this year, and will return in next March. We expect to observe auroral data at high-latitude in February and March 2022 and will examine the data after Shirase's return in Spring of 2022.

Citizen science of aurora hunting in Japan: Evidence of red aurora on October 12, 2021

Ryuho Kataoka[1], Satoru Fukushima[2], Yasuo Sano[3] and Kouki Tamura[4]
[1]*National Institute of Polar Research*
[2]*Amatuer astronomer 1*
[3]*Amatuer astronomer 2*
[4] *Amatuer astronomer 3*

We show the best example of the most recent auroral citizen science on October 12, 2021, when we had a moderate magnetic storm (real-time Dst peak of −53 nT at 1500–1600 UT). The real-time AE index was, however, extreme, reaching ~2500 nT at 1100–1130 UT. The solar wind driver was likely a complex ejecta without clear signature of magnetic flux rope, possibly separating the sheath and body by the discontinuity at ~0900 UT. The solar wind speed after the interplanetary shock at 0145 UT were rather stable at ~450 km/s with intermittent strong (~15 nT) souwthward Bz. Most notably, the solar wind density was quite high at >30 /cc. The solar origin was the M1.6 flare ocurred at around disk center at 0620–0630 UT on October 9, 2021 and the associated halo coronal mass ejection.

At that night (1200–1600 UT, or 2100–2500 JST), red auroras appeared around the north horizen (~10 deg elevation angle) were successfully photographed by citizens living in northern part of Hokkaido, Japan (magnetic latitude was ~36 deg with geographic coordinates of 44–45N and 142E). 1200–1600 UT was 22–02 MLT sector at 50 deg magentic latitude in this longitude. This is surprising evidence that the auroral oval at magnetic midnight possibly extended down to ~46 deg after the super substorm for ~4 hours, with little enhancement of the ring current. The large oval extension was also supported by DMSP satellite data.

The trigger of this citizen science activity was Twitter (R.K. has ~13K Japanese followers). R.K. reported the professional space weather forecast of magnetic storms real-time, and indicated the possibility to hunt auroras from Hokkaido, Japan in advance. Several citizens watched the tweets and succeeded to photograph the northern red sky, and kindly reported via twitter and provided those photos via emails for this citizen science research. This study implies that Japanese citizens are high level as amatuer astronomers and ready in this form to contribute for studying upcoming extreme magnetic storms.

ANGWIN: ANtarctic Gravity Wave Instrument Network

T. Moffat-Griffin[1], T. Nakamura[2], J. V. Bageston[3], D. J. Murphy[4], G. Jee[5] and M. J. Taylor[6]
[1]*British Antarctic Survey, Cambridge, United Kingdom*
[2]*National Institute of Polar Research, Tachikawa, Japan*
[3]*National Institute for Space Research INPE, São José Dos Campos, Brazil*
[4]*Australian Antarctic Division, Kingston, Australia*
[5]*Korea Polar Research Institute, Incheon, Korea*
[6]*Utah State University, Logan, USA*

Atmospheric gravity waves play an important role in transporting energy and momentum between atmospheric spheres and drive circulations that affect key processes such as the formation of the ozone hole and the cold summer polar mesosphere. The lack of comprehensive observations over the Antarctic region has an impact on our understanding of these processes. The ANtarctic Gravity Wave Instrument Network (ANGWIN) is a highly successful grassroots programme that was started in 2011. It seeks to use a network of observations to measure gravity waves continent wide and through all levels of the atmosphere, in order to fully understand their impact and to constrain modelling work.

Although ANGWIN initially focused on the Antarctic, the group is now aiming to develop collaborations in both polar regions. Current member countries of ANGWIN are Australia, Brazil, Canada, Japan, South Korea, the United Kingdom and the United States of America. Antarctic and sub-Antarctic stations contributing to the ANGWIN network are shown in Figure 1.

The objective of ANGWIN network include;

- Quantify the longitudinal variations in gravity waves and determine causes;
- Characterize wave propagation and influence;
- Relate observed gravity waves to sources throughout the atmosphere;
- Study interactions of gravity waves with planetary scale waves;
- Compare polar wave observations to model parameterizations;
- Determine the effects of gravity waves on polar stratospheric cloud formation.

ANGWIN researchers have met in workshops held in Tokyo, Japan (2013), Logan, USA (2014), Cambridge UK (2016) and São José dos Campos, Brasil (2018). A special issue of the Journal of Geophysical Research includes publications from ANGWIN related studies (see https://doi.org/10.1029/2019JD030247).

This presentation will provide an update on current ANGWIN activities and highlight recent studies of polar gravity waves.

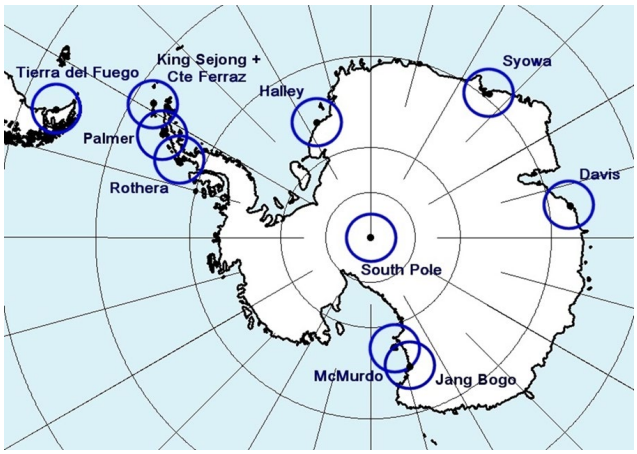

Figure 1. Antarctic stations contributing to ANGWIN observations.

References

Information about the SCAR ANGWIN Action group can be found at https://www.scar.org/science/angwin/home/

Polar mesospheric cloud detection by the Advanced Himawari Imager onboard the Japanese geostationary-Earth-orbit meteorological satellite Himawari-8

T. T. Tsuda[1], Y. Hozumi[2], Y. Ando[1], K. Hosokawa[1], H. Suzuki[3], K. T. Murata[2],
T. Nakamura[4,5], J. Yue[6], K. Nielsen[7], and Y. Miyoshi[8]

[1]*Department of Computer and Network Engineering, University of Electro-Communications (UEC), Chofu, Japan*
[2]*National Institute of Information and Communications Technology (NICT), Koganei, Japan*
[3]*Department of Physics, Meiji University, Kawasaki, Japan*
[4]*National Institute of Polar Research (NIPR), Tachikawa, Japan*
[5]*Department of Polar Science, Graduate University for Advanced Studies (SOKENDAI), Tachikawa, Japan*
[6]*Goddard Space Flight Center (GSFC), National Aeronautics and Space Administration (NASA), Greenbelt, US*
[7]*Department of Physics, Utah Valley University (UVU), Orem, US*
[8]*Department of Earth and Planetary Sciences, Kyushu University, Fukuoka, Japan*

With the objective of advancing the polar mesospheric cloud (PMC) detection capability by the Advanced Himawari Imager (AHI) onboard the Japanese geostationary-Earth-orbit (GEO) meteorological satellite Himawari-8, a novel two-step PMC detection technique applied towards the Himawari-8/AHI full-disk images has been developed. The two-step approach is dividing the PMC detection into stronger (the first step) and weaker (the second step) signals and enhances the detection capability while significantly decreasing the false PMC detections. The improved PMC sensitivity by Himawari-8/AHI is comparable with the Cloud Imaging and Particle Size (CIPS) onboard the Aeronomy of Ice in the Mesosphere (AIM) satellite. With this encouraging result, PMC observations from Himawari-8/AHI provide an additional extensive data set to the aeronomy and space science community.

Development of image correction system for the all-sky imager onboard Antarctic Research Vessel "Shirase"

Saki Yamashina[1], Akinori Saito[1], Takeshi Sakanoi[2] , Yuta Hozumi[3], Takuo T.Tsuda[4], Takeshi Aoki[4], Takahiro Naoi[3], Masato Nagahara[3], Mitsumu K.Ejiri[5], Takanori Nishiyama[5]

[1]*Kyoto University,* [2]*Planetary Plasma and Atmospheric Research Center, Graduate School of Science, Tohoku University,* [3]*NICT,* [4]*The University of Electro-Communications,* [5]*NIPR*

Ground-based imagers have been used for optical ionospheric and mesospheric observations [e.g., Shiokawa et al., 1999]. While imager networks are expanding for these three decades [e.g., Mende et al., 2008], there are observational gaps especially in the southern hemisphere, where the ocean occupies a large proportion of the area. To fill these gaps, we conducted optical ionospheric observations using a vessel-borne all-sky imager. The optical observations with the vessel-borne imagers are affected by the movement and vibration of the vessel. The objective of this study is to develop efficient methods to correct images captured by the vessel-borne imagers. All-sky imagers were installed on the Antarctic research vessel "Shirase" during the 61st Japanese Antarctic Research Expedition (JARE 61) and JARE 62. On the outbound trip of JARE 61, observations were carried out for 51 days (from November 11 to December 31, 2019), and airglow was successfully observed since the vessel passed under the equatorial anomaly zone. On the return trip of JARE 61, observations were carried out for 42 days (from February 7 to March 19, 2020), and auroras were successfully observed since the vessel traveled east-west under the southern auroral zone for a long time. On the outbound and return trip of JARE 62, observations were carried out for 22 days (from November 20 to December 11, 2020) and 33 days (from January 25 to February 26, 2021), respectively. An unusual route was chosen in JARE 62 due to the influence of Covid-19. In JARE 61, an imager was equipped with an interference filter whose central wavelength is 630 nm, and the exposure time was set to 18 s. In JARE 62, two imagers were equipped with interference filters whose central wavelengths are 630 nm and 670 nm, respectively, and the exposure time was set to 9s. The imagers were mounted on a 3-axis attitude stabilized gimbal, which cancels the vessel's vibration. If the vessel's vibration is shorter than the exposure time, the vibration is canceled by the gimbal. On the other hand, if the vessel's vibration is sufficiently longer than the exposure time, the gimbal follows the vibration, and then the imager changes its orientation. Although the imager's shooting direction can be determined from the position of the stars in the images, this is limited to images taken in clear weather. Therefore, we determined the imager's orientation by obtaining the relative angle between the imager and the vessel. The relative angle was obtained by automatically detecting the vessel's structure in the captured images. By combining the relative angle with the attitude data of "Shirase", a system to automatically detect the shooting direction was developed. The accuracy of the direction estimation was evaluated by comparing it with the shooting direction determined from the position of the stars in the images, and it was found that the maximum error was about 3 degrees. This is equivalent to about 13 km on the horizontal scale at an altitude of 250 km if a zenith angle is 45 degrees, and it is sufficiently small compared to the horizontal scale of aurora and airglow.

References

Shiokawa, K., et al., Development of Optical Mesosphere Thermosphere Imagers (OMTI), Earth Planets Space, 51, 887–896, 1999.

Mende, S. B., et al., The THEMIS Array of Ground-based Observatories for the Study of Auroral Substorms, Space science reviews, 141, 357–387, 2008.

Characteristics of 8 hr and 6 hr atmospheric waves in the polar upper mesosphere and lower thermosphere derived by the sodium LIDAR at Tromsø

Chiaki Morikawa[1], Satonori Nozawa[1], Takuo T. Tsuda[2], Takuya Kawahara[3], Norihito Saito[4], Satoshi Wada[4], Toru Takahashi[5], and Tetsuya Kawabata[1]

[1]*ISEE, Nagoya University*

[2]*Department of Communication Engineering and Informatics, The University of Electro-Communications*

[3]*Faculty of Engineering, Shinshu University*

[4]*RIKEN Center for Advanced Photonics, RIKEN*

[5]*Electronic Navigation Research Institute*

We will report characteristics of 8 hr and 6 hr atmospheric waves observed in the polar upper Mesosphere and Lower Thermosphere (MLT) region over 7 years between 2012 and 2019 at Tromsø, Norway (69.6 ºN, 19.2 ºE). Wind velocity and temperature data obtained by the sodium lidar at Tromsø have been used to analyze these waves. Even though an amplitude of the 8 hr tide becomes sometimes comparable to that of 24 hr tidal wave in the polar MLT region [Thayaparan, 1997; Younger et al., 2002], 8 hr and 6 hr tidal waves are poorly known in comparison with 24 hr and 12 hr tidal waves. Solar heating and nonlinear interactions of 24 hr and 12 hr tides are considered to generate the 8 hr tide [Thayaparan, 1997; Akmaev, 2001; Younger et al., 2002; Moudden et al., 2013]. A previous modeling study showed that solar heating was a dominant factor of 8 hr tide generations at high latitudes [Smith, 2001]. Pancheva et al. [2021] using meteor radar wind data at Tromsø showed that both 8 hr and 6 hr tides had inter annual variability with a quasi-2-year-period, and vertical upward propagating of these waves had different wavelength according to season. They showed the 8 hr tide in November has a long vertical wavelength (larger than 100 km).

In this talk, we will present characteristics of 8 hr and 6 hr periodic atmospheric waves using both temperature and wind velocity data between 80 and 110 km. We have analyzed 8 hr waves for 90 nights and 6 hr waves for 125 nights. Vertical wavelengths of them are also derived to discuss their generations: The 8 hr waves have wavelengths of about 10 - 40 km. We will also report relative importance of these waves to the 12 hr wave.

References

Akmaev, R. A., Seasonal variations of the terdiurnal tide in the mesosphere and lower thermosphere: A model study, Geophysical Research Letters, 28, 3817–3820, https://doi.org/10.1029/2001GL013002, 2001.

Moudden, Y., and J. M. Forbes, A decade-long climatology of terdiurnal tides using TIMED/SABER observations, Journal of Geophysical Research: Space Physics, 118, 4534–4550, https://doi.org/10.1002/jgra.50273, 2013

Pancheva, D., P. Mukhtarov, C. Hall, A.K. Smith, M.Tsumi, Climatology of the short-period (8-h and 6-h) tides observed by meteor radars at Tromsø and Svalbard, Journal of Atmospheric and Solar Terrestrial Physics, 212, 105513, https://doi.org/10.1016/j.jastp.2020.105513, 2021

Smith, A.K., and D. A. Ortland, Modelling and analysis of the structure and generation of the terdiurnal tide, Journal of the Atmosphere Sciences, 5, 3116–3134, 2001.

Thayaparan, T., The terdiurnal tide in the mesosphere and lower thermosphere over London, Canada (43 deg N,81 deg W), Journal of Geophysical Research, 102, 21,695–21,708, 1997.

Younger, P.T., D. Pancheva, D. Middleton, H. R., and Mitchell, N. J, The 8-hour tide in the Arctic mesosphere and lower thermosphere. Journal of Geophysical Research, 107(A12), 1420. https://doi.org/10.1029/2001JA005086, 2002.

A long lived mesospheric Ca^+ ion layer observed by a resonance scattering lidar at Syowa

Mitsumu K. Ejiri[1,2], Takanori Nishiyama[1,2], Takuo T. Tsuda[3], Masaki Tsutsumi[1,2], Takuji Nakamura[1,2], Katsuhiko Tsuno[4], Makoto Abo[5], Takuya D. Kawahara[6], Takayo Ogawa[4], Satoshi Wada[4]

[1]*National Institute of Polar Research, Midoricho 10-3, Tachikawa, Tokyo 190-8518, Japan.*
[2] *Department of Polar Science, The Graduate University for Advanced Studies, SOKENDAI, 10-3 Midoricho, Tachikawa, Tokyo, Japan.*
[3]*The University of Electro-Communications, 1-5-1 Chofugaoka, Chofu, Tokyo 182-8585, Japan.*
[4]*RIKEN, RAP, 2-1 Hirosawa, Wako, Saitama 351-0198, Japan.*
[5]*Tokyo Metropolitan University, Asahigaoka 6-6, Hino-shi, Tokyo 191-0065, Japan.*
[6]*Shinshu University Faculty of Engineering, 4-17-1 Wakasato, Nagano 380-8553, Japan.*

Metal atoms and ions in the mesosphere and lower thermosphere (MLT) are sourced from meteoric ablation. The meteoric metal ions have relatively long chemical lifetime in the MLT and behave as a plasma affected by neutral atmosphere dynamics. Ca^+ ion is only meteoric metal ion can be observed by a ground-based resonance scattering lidar with high time and height resolution. The Ca^+ lidar measurements have been carried out at the mid and low latitudes. Annual variation of the Ca^+ vertical distribution observed at Kühlungsborn in 1997-1998 showed existing a permanent Ca^+ layer between 90 and 100 km through the year though it was sometimes rather weak (Gerding et al., 2000). Raizada et al. (2012) showed that average Ca^+ density below 95 km altitude in summer was larger than in winter over Arecibo though the Ca^+ chemical lifetimes below 95 km during summer, ~2–20 minutes, was shorter as compared to winter, ~8–30 minutes. Therefore, they concluded that the variations in Ca^+ distribution and concentrations on the seasonal scale were governed more by the dynamics rather than the loss processes due to neutralization. However, the effect of the fast neutralization on time-height distribution of Ca^+ ion on a night is still under investigation.

A resonance scattering lidar system with frequency-tunable alexandrite laser was developed by the National Institute of Polar Research (NIPR) and installed at Syowa Station (69S, 40E) by the 58th Japan Antarctic Research Expedition (JARE 58). Density profiles of Ca^+ in the MLT region over Antarctic were successfully observed 6 nights in total in September and October, 2017 and 2018. On October 6, 2018, a Ca^+ thin layer staying around 92 km altitude more than 3 hours was observed. That night was very quiet geomagnetic conditions according to the geomagnetic data at Syowa, therefore contribution of electric fields to the Ca^+ layer formation and change was negligible. The vertical Ca^+ ion drift velocity due to vertical shear of horizontal neutral winds can be estimated using wind measurements by the MF radar at Syowa. The estimated vertical ion velocities show no ion convergence around the Ca^+ thin layer but may cause to change the layer altitudes. In this presentation, we will discuss contributions of dynamics and chemical process to the observed time-height change of the Ca^+ thin layer using the vertical ion velocity and the Ca^+ chemical lifetime at the polar region; calculated with neutral atmosphere densities (O, O_2, N_2, He) and temperature from the NRLMSIS-00 atmosphere model, minor constituent densities (CO_2, O_3, H_2O) from the MIPAS model atmosphere, and electron density from the International Reference Ionosphere (IRI) model.

References

Gerding, M., M. Alpers, U. von Zahn, R. J. Rollason, and J. M. C. Plane (2000), The atmospheric Ca and Ca+ layers: Midlatitude observations and modeling, J. Geophys. Res., 105, 27,131–27,146, doi:10.1029/2000JA900088.

Raizada, S., C. A. Tepley, B. P. Williams, and R. García (2012), Summer to winter variability in mesospheric calcium ion distribution and its dependence on Sporadic E at Arecibo, J. Geophys. Res., 117, A02303, doi:10.1029/2011JA016953.